Multiringed breathers and rotating breathers in strongly nonlocal nonlinear media under the off-waist incident condition

Daquan Lu and Wei Hu*
Laboratory of Photonic Information Technology, South China Normal University, Guangzhou 510631, China
(Received 29 December 2008; published 29 April 2009)

We introduce two classes of spatial optical breathers in strongly nonlocal nonlinear media: multiringed breathers and rotating breathers, which can be created as results of the superposition of off-waist input Laguerre-Gaussian beams. Their width "breathes" sinusoidally during propagation under the off-waist incident condition, whatever the input power is. Only when the beam is inputted at the waist and the input power equals the critical power simultaneously would the multiringed (rotating) breather reduce to a multiringed (rotating) soliton. For a rotating breather, the azimuthal orientation of the intensity pattern is determined by the indices of the constituent beams and varies periodically in propagation. This property together with the breath of the beam width yields novel trajectories which the points within the beam cross section undergo.

DOI: 10.1103/PhysRevA.79.043833 PACS number(s): 42.65.Tg, 42.65.Jx

I. INTRODUCTION

The nonlocal nonlinearity, which is featured by many physical systems such as plasmas [1], Bose-Einstein condensates [2], and some optical materials [3–8], has attracted considerable interest in recent years. The nonlocality plays an important role in the nonlinear evolution of waves. It has been shown that there are some particular properties induced by the nonlocality, such as the suppression of collapse [9] and the support of vortex solitons [10,11] and multipole solitons [12]. In nonlinear optics especially, the nonlocality was found in materials such as nematic liquid crystal [3,4] and lead glass [5,6]. In these materials, the characteristic length of the material response function can be much larger than the beam width; and they are called strongly nonlocal nonlinear (SNN) media (or equivalently, highly nonlocal nonlinear media). In the SNN condition, the governing equation, i.e., the nonlocal nonlinear Schrödinger equation, can be simplified to a linearized equation tantamount to the equation for the two-dimensional harmonic oscillator [called the Snyder-Mitchell model (SMM) here] [13]:

$$2ik\partial_z A + (\partial_{xx} + \partial_{yy})A - k^2\gamma^2 P_0 r^2 A = 0, \tag{1}$$

where k is the wave vector in a linear medium, γ is a material constant, and $P_0 = \int |A|^2 d^2\mathbf{r}$ is the input power, with $\mathbf{r} = (x, y)$.

Quite different from the conventional standard local Kerr-type material which supports only (1+1)D spatial or temporal solitons, the SNN media support not only (2+1)D spatial solitons, but also (2+1)D spatial breathers, whose pattern shape remains invariant and whose width "breathes" sinusoidally during propagation. In fact, since Snyder and Mitchell [13] introduced the SMM to investigate the propagation in SNN media and found that it supports the so-called accessible solitons [13], various structures of solitons and breathers [10–23], such as multivortex solitons [11], multipole solitons [12], azimuthons [16], and ellipticons [21], have been theoretically predicted. Some of them have been observed experimentally [3–7].

We note that the solitons and breathers in above-mentioned papers are theoretically predicted under the assumption that the beams are inputted at the beam waist. In contrast the off-waist input case remains unexplored. In this paper, we introduce two classes of SNN spatial optical breathers under the off-waist incident condition: multiringed breathers and rotating breathers. It is revealed that the propagation of the off-waist incident multiringed beams in SNN media yields multiringed breathers, and the combination of two off-waist incident multiringed breathers with different indices yields SNN rotating breathers. The beam width and phase distribution of multiringed breathers and rotating breathers vary periodically during propagation, whatever the input power is. Only when the beams are inputted at the waist and the input power equals the critical power simultaneously would multiringed breathers and rotating breathers reduce to multiringed solitons and rotating solitons, respectively. For rotating breathers, every point within the beam cross section undergoes novel trajectory, because the breath of the beam width is dependent on the periodically varied azimuthal orientation of the intensity pattern.

II. MULTIRINGED BREATHERS UNDER THE OFF-WAIST INCIDENT CONDITION

A. Analytical solution

We consider the SNN propagation of multiringed shape-invariant beam which is transmitted from free space into SNN media under the off-waist incident condition. The entrance plane is supposed to be situated at $z=0$, and the beam waist is assumed to be located at $z=z_s$.

In free space, a shape-invariant multiringed beam can be formed by superposition of an even and an odd Laguerre-Gaussian beam with identical parameters except for a $\pm\pi/2$ phase difference between them, i.e.,

*huwei@scnu.edu.cn

$$\Psi_{pl}(r,\varphi,z) = A_0(\mathcal{L}_{pl}^{e} \pm i\mathcal{L}_{pl}^{o}) = A_0\frac{w_0}{w_f}\left(\frac{r}{w_f}\right)^{|l|} L_p^{|l|}\left(\frac{r^2}{w_f^2}\right) \times \exp\left(-\frac{r^2}{w_f^2}\right)\exp\left(\frac{ikr^2}{2R_f} - i\psi_f + il\varphi\right), \quad (2)$$

where the coefficient A_0 is related to the input power P_0 through $P_0=\int|\Psi_{pl}(r,\varphi,z)|^2 d^2\mathbf{r}$,

$$\mathcal{L}_{pl}^{e,o} = \frac{w_0}{w_f}\left(\frac{r}{w_f}\right)^{|l|} L_p^{|l|}\left(\frac{r^2}{w_f^2}\right)\exp\left(-\frac{r^2}{w_f^2}\right)\exp\left(\frac{ikr^2}{2R_f} - i\psi_f\right) \times \begin{cases}\cos(|l|\varphi)\\ \sin(|l|\varphi),\end{cases} \quad (3)$$

$w_f(z)=w_0[1+(z-z_s)^2/z_0^2]^{1/2}$, $R_f(z)=(z-z_s)[1+z_0^2/(z-z_s)^2]$, $\psi_f(z)=(2p+|l|+1)\arctan[(z-z_s)/z_0]$, $z_0=kw_0^2$, φ is the azimuthal angle, $p,|l|=0,1,2,\ldots$, and $L_p^{|l|}(\cdot)$ represents the generalized Laguerre polynomial.

The evolution of multiringed beams in SNN media can be obtained by solving the SMM, i.e., Eq. (1). In our previous work [24], we have introduced a one-to-one correspondence between the beam solution of free propagation and that of SNN propagation based on the relationship between Eq. (1) and the diffraction equation which governs the free propagation:

$$A(\mathbf{r},z) = F_1F_2\Psi(F_1\mathbf{r},F_3), \quad (4)$$

where

$$F_1(z) = (-1)^a\left[1+\tan^2\left(\frac{z}{z_{p0}}\right)\right]^{1/2},$$

$$F_2(\mathbf{r},z) = \exp\left\{-\frac{ikF_1(z)^2r^2}{2z_{p0}\left[\tan\left(\frac{z}{z_{p0}}\right)+1/\tan\left(\frac{z}{z_{p0}}\right)\right]}\right\},$$

$$F_3(z) = z_{p0}\tan\left(\frac{z}{z_{p0}}\right),$$

$$a(z) = \frac{1}{\pi}\left\{\frac{z}{z_{p0}} - \arctan\left[\tan\left(\frac{z}{z_{p0}}\right)\right]\right\},$$

$$z_{p0} = (\gamma^2P_0)^{-1/2}. \quad (5)$$

A and Ψ represent the beam solution of free propagation and that of SNN propagation, respectively.

Substituting Eq. (2) into Eq. (4) yields the solution of the off-waist input multiringed beam in SNN media:

$$A_{pl}(r,\varphi,z) = A_0\frac{w_0}{w}\left[\frac{(-1)^a r}{w}\right]^{|l|} L_p^{|l|}\left(\frac{r^2}{w^2}\right) \times \exp\left(-\frac{r^2}{w^2}\right)\exp\left[\frac{ikr^2}{2R} - i\psi(z) + il\varphi\right], \quad (6)$$

where

$$w(z) = \frac{w_0\left\{1+\left[\frac{z_{p0}}{z_0}\tan\left(\frac{z}{z_{p0}}\right)-\frac{z_s}{z_0}\right]^2\right\}^{1/2}}{\left[1+\tan^2\left(\frac{z}{z_{p0}}\right)\right]^{1/2}},$$

$$R_c(z) = \frac{1}{1+\tan^2\left(\frac{z}{z_{p0}}\right)}\frac{1}{\frac{1}{\left[z_{p0}\tan\left(\frac{z}{z_{p0}}\right)-z_s\right]\left\{1+1/\left[\frac{z_{p0}}{z_0}\tan\left(\frac{z}{z_{p0}}\right)-\frac{z_s}{z_0}\right]^2\right\}} - \frac{1}{z_{p0}\tan\left(\frac{z}{z_{p0}}\right)\left[1+1/\tan\left(\frac{z}{z_{p0}}\right)^2\right]}},$$

$$\psi(z) = (2p+|l|+1)\left\{a\pi + \arctan\left[\frac{z_{p0}}{z_0}\tan\left(\frac{z}{z_{p0}}\right)-\frac{z_s}{z_0}\right]\right\}. \quad (7)$$

It is noted that z_{p0} is determined by the input power P_0 and plays an important role in the evolution of the field in SNN media.

As shown in Eq. (6), during SNN propagation the multiringed beams are shape invariant and the beam width as well as the phase distribution varies periodically with the period

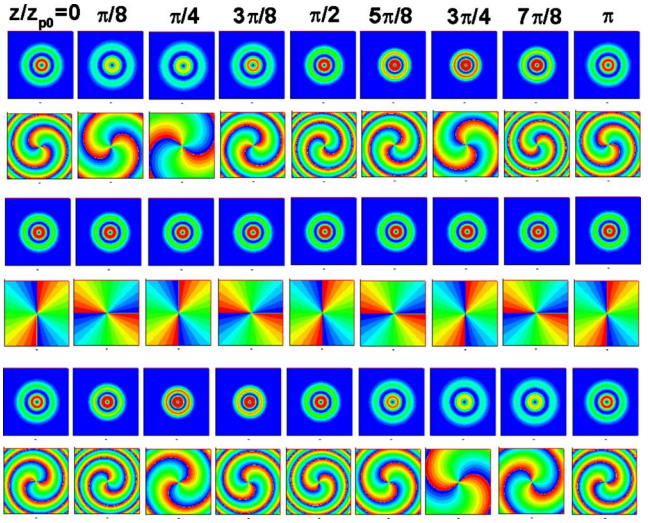

FIG. 1. (Color online) Evolutions of intensity distribution (rows 1, 3, and 5) and phase distribution (rows 2, 4, and 6) of the (1,1) mode multiringed breather for different off-waist distances. The off-waist distances are $zs=-z_0/2$ (rows 1 and 2), 0 (rows 3 and 4), and $z_0/2$ (rows 5 and 6); $P_0=P_c$.

$\Delta z=\pi z_{p0}$ (Fig. 1). Thus we call these beams the multiringed breathers. For a multiringed breather with the indices (p,l), there are $|l|$ circular nodal lines in the pattern, and the number of rings is $|l|+1$. In (r,φ) plane, the phase clockwise (anticlockwise) increases by $2|l|\pi$ in an azimuthal circuit if $l<0$ $(l>0)$.

B. Evolution of the beam width

In propagation, the parameter w in Eq. (7) represents the second-order moment width of the (0,0) mode breather, and that of a higher-order multiringed breather is $\sqrt{2p+l+1}w(z)$. As shown in Eq. (7), the width of the multiringed breathers varies periodically with the period πz_{p0} in propagation.

When the width reaches its maximum or minimum, we have

$$\partial_z w^2(z) = \frac{2z_s z_{p0} + \cos\left(\frac{2z}{z_{p0}}\right) + (z_0^2 - z_{p0}^2 + z_s^2)\sin\left(\frac{2z}{z_{p0}}\right)}{z_0^2 z_{p0}} = 0, \tag{8}$$

the solution of which is

$$z_m^{(n)} = \frac{z_{p0}}{2}\left[n'\pi + \arctan\left(\frac{2z_{p0}z_s}{-z_0^2 + z_{p0}^2 - z_s^2}\right)\right], \tag{9}$$

where $z_m^{(n)}$ represents the nth cross sections at which the width reaches its maximum or minimum, $n'=n$ $(n'=n-1)$ if $z_s>0$ $(z_s<0)$. Equation (9) shows that $z_m^{(n)}$ is proportional to z_{p0}, and the spacing between $z_m^{(n)}$ and $z_m^{(n+1)}$ is $\pi z_{p0}/2$. In the following, for convenience of discussion, we describe these cross sections with a normalized parameter $Z_m^{(n)}$, which is defined as

$$Z_m^{(n)} = \frac{z_m^{(n)}}{z_{p0}} = \frac{1}{2}\left[n'\pi + \arctan\left(\frac{2z_{p0}z_s}{-z_0^2 + z_{p0}^2 - z_s^2}\right)\right]. \tag{10}$$

In propagation, the beam alternately focuses and diffracts. The focusing (diffracting) can be determined through the inequation $\partial_z w^2<0$ $(\partial_z w^2>0)$. For convenience of discussion, we introduce the critical power P_c, which is defined as

$$P_c = (z_0\gamma)^{-2}.$$

When the beam is inputted at the beam waist, it can present itself as breather or soliton [Fig. 2(b)]. If the input power $P_0<P_c$ $(P_0>P_c)$, the beam width increases (decreases) first because the focus is weaker (stronger) than the diffraction; then it increases and decreases alternately in propagation. If $P_0=P_c$, the diffraction is balanced by the focusing. Thus the beam width is kept invariant during propagation and the breather reduces to a soliton.

On the other hand if the beam is inputted under the off-waist condition, i.e., $z_s\neq 0$, it is impossible for the breather to reduce to a soliton [Figs. 2(a) and 2(c)]. When $z_s<0$ $(z_s>0)$, due to the convex (concave) cophasal surfaces at the entrance plane, the beam width first increases (decreases) until it reaches its maximum (minimum), and then it increases and decreases alternately, whatever the input power is.

If the off-waist distance z_s is fixed and the input power is changed (Fig. 2), (i) the average beam width decreases with the input power, because a higher input power provides a stronger self-focusing effect; and (ii) every $Z_m^{(n)}$ varies with the input power. When $z_s>0$ $(z_s<0)$, every $Z_m^{(n)}$ increases (decreases) with the input power. If the power is high enough so that $z_{p0}\ll z_0$, the first normalized minimum-width plane would approach $\pi/2$.

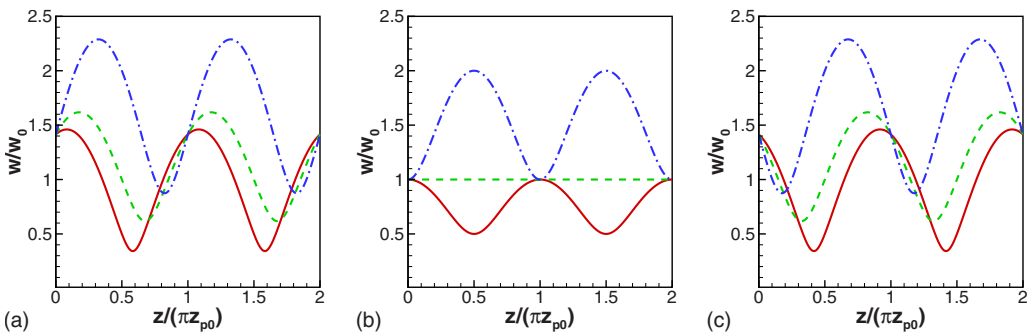

FIG. 2. (Color online) (a) Evolutions of the beam width for different input powers when $z_s=-z_0$; the input powers are $P_0=4P_c$ (solid line), P_c (dashed line), and $0.25P_c$ (dash-dotted line). (b) The same as (a) except $z_s=0$. (c) The same as (a) except $z_s=z_0$.

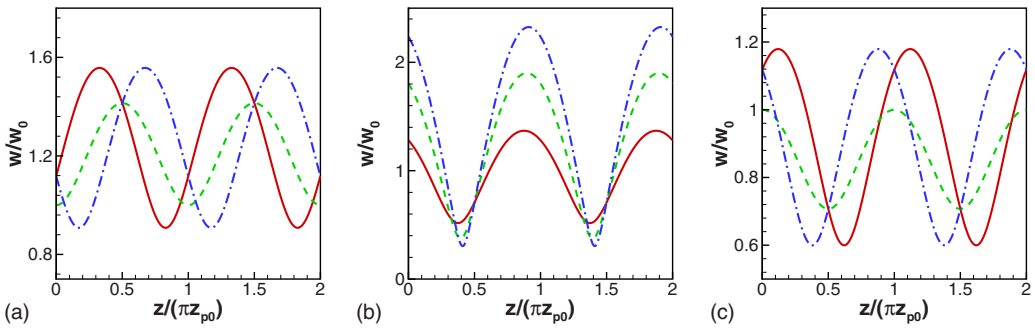

FIG. 3. (Color online) (a) Evolutions of the beam width for different off-waist distances z_s when $P_0=0.5P_c$. The off-waist distances are $z_s=-0.5z_0$ (solid line), 0 (dashed line), and $0.5z_0$ (dash-dotted line). (b) Evolutions of the beam width for different off-waist distances z_s when $P_0=2P_c$. The off-waist distances are $z_s=0.8z_0$ (solid line), $1.5z_0$ (dashed line), and $2z_0$ (dash-dotted line). (c) The same as (a) except $P_0=2P_c$.

If the input power is fixed and the off-waist distance z_s is changed (Fig. 3), (i) the average beam width increases with $|z_s|$; (ii) the average beam width for z_s is the same as that for $-z_s$, because $w(z)|_{z_s=+|z_s|}=w(-z)|_{z_s=-|z_s|}$, as shown in Eq. (7); and (iii) if $P_0 \leq P_c$ (or equivalently, $z_0 \leq z_{p0}$), $Z_m^{(n)}$ monotonically increases with z_s [Fig. 3(a)]. On the other hand if $P_0 > P_c$ (or equivalently, $z_0 > z_{p0}$), the variation in $Z_m^{(n)}$ with z_s is not monotonic. It decreases with z_s if

$$-(z_0^2 - z_{p0}^2)^{1/2} < z_s < (z_0^2 - z_{p0}^2)^{1/2}$$

[Fig. 3(c)]; otherwise it increases with z_s [Fig. 3(b)]. (iv) Although the beam widths at the entrance plane are different for different off-waist shifts, they are equal to each other at the planes $z=(n+1/2)\pi z_{p0}$. The reason is that the fields at these planes are the $2n+1$ times of Fourier transform (or, in other words, the angular spectrum) of the fields at the entrance planes, which are the same for different off-waist shifts.

C. Evolution of the phase distribution

The evolution of the phase is composed of three parts: (i) the azimuthal variation in the phase, $il\varphi$, which results in $2|l|\pi$ anticlockwise (clockwise) increase in the phase in an azimuthal circuit in (r,φ) plane if $l>0$ ($l<0$); (ii) the Gouy phase shift $i\psi(z)$; and (iii) the radial variation in the phase, $ikr^2/2R(z)$, which is caused by the variation in the radius of cophasal surfaces, $R(z)$. In propagation, the combination of the above-mentioned three parts would result in a novel evolution of the phase distribution, as will be discussed in the following.

The evolution of the radius of cophasal surfaces, $R(z)$, plays an important role in the evolution of the phase distribution of the multiringed breathers. Before studying the evolution of the phase distribution, it is constructive to discover the relationship between the evolution of the radius of cophasal surfaces, $R(z)$, and the beam width $w(z)$.

Substituting Eq. (9) into the expression for $R(z)$ in Eq. (7) yields

$$R(z_m^{(n)}) = \pm\infty, \tag{11}$$

which means that the cophasal surfaces become plane ones when the beam width reaches its maximum or minimum.

Between a maximum-beam-width plane and the contiguous minimum-beam-width plane, there is a plane $z_{\min\ R}$ where $|R(z)|$ reaches its minimum $|R|_{\min}$, which can be obtained from the equation $\partial_z R(z)=0$, yielding

$$z_{\min\ R} = n\pi z_{p0} + z_{p0} \arctan\left\{ \frac{z_0^4 - z_0^2(z_{p0}^2 - 2z_s^2) + z_s^2(z_{p0}^2 + z_s^2)}{z_{p0}[z_0^2 z_s + z_{p0}^2 z_s + z_s^2 \pm z_0\sqrt{z_0^4 - 2z_0^2(z_{p0}^2 - z_s^2) + (z_{p0}^2 + z_s^2)^2}]} \right\}. \tag{12}$$

For convenience of discussion, we divide the propagation from a maximum-beam-width plane to the next one into four parts (Fig. 4). (i) In propagation from a maximum-beam-width plane to the contiguous $z=z_{\min\ R}$ plane, R monotonically increases from $-\infty$ to $-|R|_{\min}$. (ii) In propagation from the $z=z_{\min\ R}$ plane to the contiguous minimum-beam-width plane, R monotonically decreases from $-|R|_{\min}$ to $-\infty$. (iii) In propagation from the minimum-beam-width plane to the contiguous $z=z_{\min\ R}$ plane, R monotonically decreases from $+\infty$ to $+|R|_{\min}$. (iv) In propagation from the $z=z_{\min\ R}$ plane to the contiguous maximum-beam-width plane, R monotonically increases from $+|R|_{\min}$ to $+\infty$.

Because the cophasal surfaces are curved and the radius of cophasal surfaces varies in propagation, the phase distribution presents a spiral form (Fig. 4). In planes where $R>0$, the cophasal lines spiral outward clockwise (anticlockwise) if $l>0$ ($l<0$). On the other hand in planes where $R<0$, the cophasal lines spiral outward anticlockwise (clockwise) if $l>0$ ($l<0$). In a word, the cophasal lines spiral outward in the opposite (same) direction as that in which the

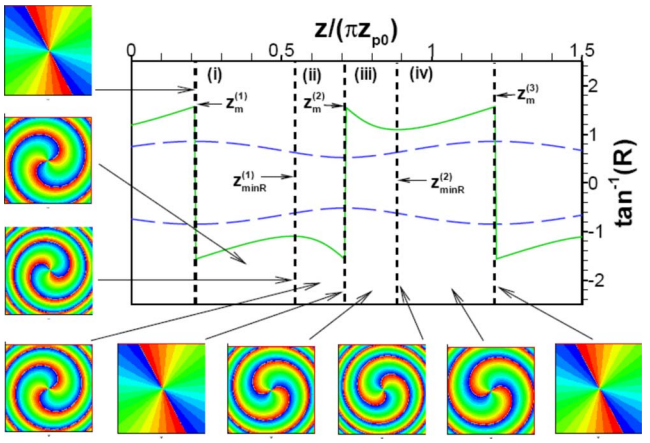

FIG. 4. (Color online) Evolutions of the radius of cophasal surfaces (solid lines), the beam profile (long-dashed lines), and phase distribution (contour maps on the left and bottom) of the (1,1) mode multiringed breather during propagation. $z_s=-z_0$; $P_0=P_c$.

phase increases when $R>0$ ($R<0$). In special case that $z_s=0$, $z_{p0}=z_0$, and the breather is reduced to a soliton, the spiral cophasal lines are reduced to straight ones (row 4 of Fig. 1), because the cophasal surfaces remains planar during propagation.

In propagation, the phase distribution is not stationary, but rotates around the propagation axis. The change in the azimuthal orientation of the phase distribution in propagation is determined by the relationship

$$\varphi(z,r)=\varphi(0,r)+\frac{\left[\psi(z)-\frac{kr^2}{2R(z)}\right]-\left[\psi(0)-\frac{kr^2}{2R(0)}\right]}{l}. \tag{13}$$

Thus the angular rotation velocity of the phase distribution is

$$\Omega^{(p)}(z,r)=\frac{d\varphi(z,r)}{dt}=\frac{c}{n_0}\frac{d\varphi(z,r)}{dz}=\frac{c}{n_0 l}\left\{\frac{kr^2R'}{2R^2}+\frac{[2p+|l|+1]\sec^2\left(\frac{z}{z_{p0}}\right)/z_0}{1+\left[\frac{z_{p0}}{z_0}\tan\left(\frac{z}{z_{p0}}\right)-\frac{z_s}{z_0}\right]^2}\right\}, \tag{14}$$

where R' represents the derivative of R with respect to z, c is the light velocity in vacuum, and n_0 is the linear part of the refractive index.

As shown in Eq. (14), the angular rotation velocity of the phase distribution is inversely proportional to l. In propagation, the angular rotation velocity of the phase distribution varies not only with the propagation distance but also with the radial location (Fig. 5). The phase distribution near the propagation axis rotates anticlockwise (clockwise) if $l>0$ ($l<0$). When $R'>0$, absolute value of the angular rotation velocity increases radially, whereas when $R'<0$ it decreases

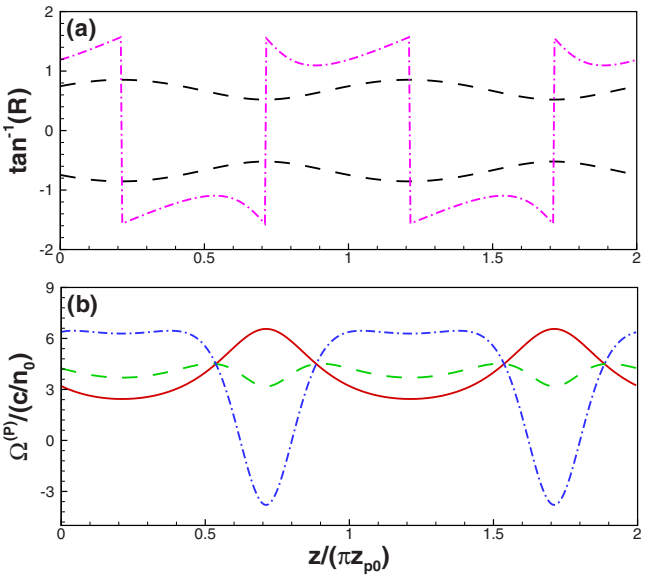

FIG. 5. (Color online) (a) Evolutions of the radius of cophasal surfaces (dash-dotted line) and the beam profile (dashed lines) of the (1,1) mode multiringed breather during propagation. (b) The longitudinal variations in angular rotation velocity of the phase distribution at $r=0.1w_0$ (solid line), $2w_0$ (dashed line), and $3.5w_0$ (dash-dotted line). In (a) and (b) $z_s=-z_0$ and $P_0=P_c$.

radially. If the transverse location is large enough, the phase distribution at the beam periphery and that near the beam axis can even rotate in opposite directions.

III. ROTATING BREATHERS UNDER THE OFF-WAIST INPUT CONDITION

A. Analytical solution

Following the approach of constructing linear azimuthons in free space [25], we assume that the field of the off-waist input rotating breathers at the entrance plane of the SNN media is

$$A^{(\mathrm{rot})}_{p1,l1,p2,l2}(r,\varphi,0)=A^{(\mathrm{rot})}_0[A^{(\mathrm{rot})}_{p1,l1}(r,\varphi,0)+bA^{(\mathrm{rot})}_{p2,l2}(r,\varphi,0)], \tag{15}$$

where $A^{(\mathrm{rot})}_0$ is related to the input power $P^{(\mathrm{rot})}_0$ through $P^{(\mathrm{rot})}_0=\int|A^{(\mathrm{rot})}_{p1,l1,p2,l2}(r,\varphi,0)|^2d^2\mathbf{r}$, and b is the weight coefficient. In free space, the combined field presents a rotation of the beam pattern in propagation if the relation

$$B=\frac{(2p_1+|l_1|)-(2p_2+|l_2|)}{l_1-l_2}\neq 0,\infty \tag{16}$$

is satisfied. Now that the free propagation is connected with the SNN propagation through a one-to-one correspondence, this existence condition is also applicable for the rotating breathers in SNN media.

In SNN propagation, the combined field induces a waveguide via the strongly nonlocal nonlinearity, and the axis of the waveguide is identical to the propagation axis of the constituent fields. The combined field in this self-induced waveguide can be readily obtained as

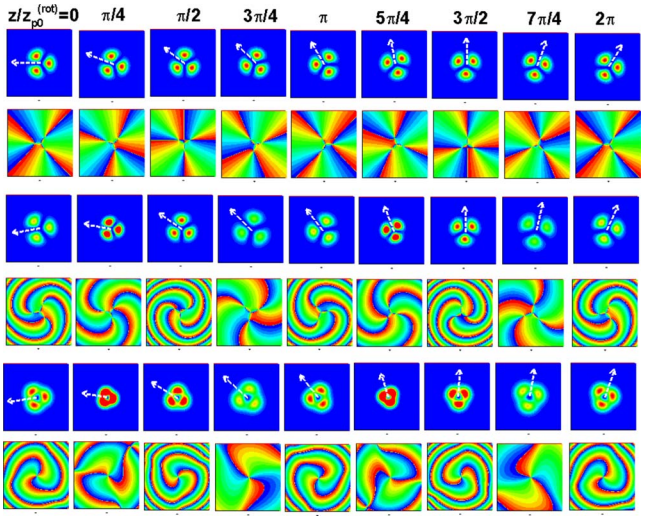

FIG. 6. (Color online) Evolutions of intensity distribution (rows 1, 3, and 5) and phase distribution (rows 2, 4, and 6) of the rotating breather $A^{(\mathrm{rot})}_{0,1,0,-2}$ with different off-waist distances z_s and different values of the weight coefficient b. The off-waist distance is $z_s=0$ for rows 1 and 2 and is $z_s=z_0/2$ for rows 3–6. The value of the weight coefficient is $b=1$ for rows 1–4 and is $b=1/7$ for rows 5 and 6. The input power is $P_0^{(\mathrm{rot})}=P_c$, which ensures $z_{p0}^{(\mathrm{rot})}=z_0$.

$$A^{(\mathrm{rot})}_{p1,l1,p2,l2}(r,\varphi,z)=A_0^{(\mathrm{rot})}[A^{(\mathrm{rot})}_{p1,l1}(r,\varphi,z)+bA^{(\mathrm{rot})}_{p2,l2}(r,\varphi,z)], \tag{17}$$

where $A^{(\mathrm{rot})}_{p,l}(r,\varphi,z)$ represents the propagated field of the constituent beams in the nonlinearity-induced waveguide by the combined field. $A^{(\mathrm{rot})}_{p,l}(r,\varphi,z)$ is the same as $A_{pl}(r,\varphi,z)$ in Eq. (6) except that the input power is not that of itself but that of the combined field, i.e., $P_0^{(\mathrm{rot})}$, and the key parameter z_{p0} is correspondingly replaced with

$$z_{p0}^{(\mathrm{rot})}=(P_0^{(\mathrm{rot})}\gamma^2)^{1/2}.$$

As will be discussed in Sec. III B, because the distribution of the phase difference between the constituent beams rotates around the axis during propagation, the pattern of the combined field rotates correspondingly. Furthermore, periodic variation in the width of constituent beams yields synchronous breath of the combined field. Therefore we call this type of beam the rotating breather.

B. Propagation properties

As shown in Fig. 6, the field of rotating breathers is determined not only by the indices of the constituent beams (i.e., p_1,l_1,p_2,l_2), but also by the weight coefficient b. The beam pattern varies with the weight coefficient b. But generally, due to azimuthal variation in the phase difference between the constituent beams, the intensity of the combined field azimuthally varies with the period $\Delta\varphi=2\pi/|l_1-l_2|$. The weight coefficient b plays an important role in the phase distribution. For example, for the rotating breather $A^{(\mathrm{rot})}_{0,1,0,-2}$, the phase in (r,φ) plane clockwise increases by 4π in an azimuthal circuit if $b=1$ (row 4), whereas it anticlockwise increases by 2π in an azimuthal circuit if $b=1/7$ (row 6). Furthermore, in propagation, the cophasal lines in the same cross section spiral outward in opposite directions for these two values of b.

Because the variation in the width of rotating breathers is synchronous to that of the constituent beams, it can be readily obtained from the results in Sec. II B, by replacing the parameter z_{p0} with $z_{p0}^{(\mathrm{rot})}$. In the rest of the subsection we focus on the rotation of the intensity distribution during propagation.

At the waist of the input field, the phase difference between the two multiringed constituent beams is $\Delta\phi_{\mathrm{waist}}=(l_1-l_2)\varphi$, which is independent of the radial position and varies azimuthally. The azimuthally varied phase difference results in a rotation-symmetric intensity pattern of the combined field. Due to difference between their Gouy phase shifts (i.e., ψ_f; readers are referred to [26,27] for detailed theory on the Gouy phase shift), the phase difference becomes $\Delta\phi(0)=[-\psi_1(0)+l_1\varphi]-[-\psi_2(0)+l_2\varphi]$ when the constituent beams are propagated from the waist to the entrance plane. Therefore the azimuthal orientation of the phase difference distribution as well as that of the pattern is varied with the angle

$$\Delta\varphi_f=[\Delta\phi(0)-\Delta\phi_{\mathrm{waist}}]/(l_1-l_2). \tag{18}$$

During SNN propagation, the difference in the SNN Gouy phase shifts (i.e., ψ) between the constituent beams results in more phase difference and yields $\Delta\phi(z)=[-\psi_1(z)+l_1\varphi]-[-\psi_2(z)+l_2\varphi]$. The azimuthal orientation of intensity pattern is rotated with the angle

$$\Delta\varphi_s=[\Delta\phi(z)-\Delta\phi(0)]/(l_1-l_2). \tag{19}$$

Therefore, in propagation the azimuthal orientation of the intensity pattern changes with the propagation distance z according to

$$\varphi(z)=\varphi_0+\Delta\varphi_f+\Delta\varphi_s=\varphi_0+aB\pi + B\arctan\left[\left(\frac{z_{p0}^{(\mathrm{rot})}}{z_0}\right)\tan\left(\frac{z}{z_{p0}^{(\mathrm{rot})}}\right)-\frac{z_s}{z_0}\right], \tag{20}$$

where φ_0 represents the azimuthal orientation of the beam pattern at the waist of the input beam. The angular rotation velocity of the pattern is

$$\Omega^{(r)}(z)=\frac{d\varphi(z)}{dt}=\frac{c}{n_0}\frac{d\varphi(z)}{dz}=\frac{\dfrac{cB}{n_0z_0}\sec^2\left(\dfrac{z}{z_{p0}^{(\mathrm{rot})}}\right)}{1+\left[\left(\dfrac{z_{p0}^{(\mathrm{rot})}}{z_0}\right)\tan\left(\dfrac{z}{z_{p0}^{(\mathrm{rot})}}\right)-\dfrac{z_s}{z_0}\right]^2}. \tag{21}$$

The beam pattern undergoes clockwise rotation in propagation when $B<0$; otherwise it undergoes anticlockwise rotation. It should be noted that the angular rotation velocity of the rotating breathers, i.e., $\Omega^{(r)}(z)$, is independent of the radial position, different from the angular rotation velocity of the phase distribution of the multiringed breathers, i.e., $\Omega^{(p)}(z)$.

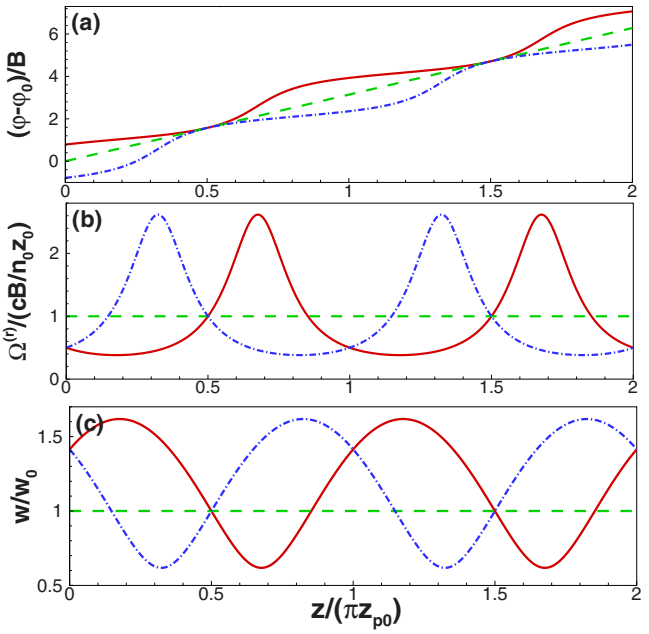

FIG. 7. (Color online) Variations in (a) the azimuthal orientation of the beam pattern, (b) the rotation velocity, and (c) the beam width with propagation for different off-waist distances. Solid lines: $z_s=-z_0$; dashed lines: $z_s=0$; dash-dotted lines: $z_s=z_0$. The input power is $P_0^{(\mathrm{rot})}=P_c$, which ensures $z_{p0}^{(\mathrm{rot})}=z_0$.

In a word, the rotation of the intensity pattern results from two factors: (i) the azimuthally varied phase difference between the constituent beams, which is determined by l_1-l_2; and (ii) the difference between the Gouy phase shifts of the two constituent beams, i.e., $\psi_1-\psi_2$, which is determined by $(2p_1+|l_1|)-(2p_2+|l_2|)$. The two factors all together influence the rotating through the key parameter B defined in Eq. (16), as shown in Eqs. (20) and (21).

As shown in Eqs. (7) and (21), both the beam width and the rotation velocity vary periodically with the period π. In fact, they are dependent on each other. The comparison between Eq. (7) and Eq. (21) yields the relationship between the beam width and the rotation velocity:

$$\Omega^{(r)}(z)=\frac{cB}{n_0 z_0}\left(\frac{w_0}{w(z)}\right)^2. \tag{22}$$

As shown in Fig. 7, (i) the rotation velocity decreases (increases) with the broadening (narrowing) of the beam, complying with the conservation of the orbital angular momentum. When the beam width reaches its maximum (minimum), the rotation velocity reaches its minimum (maximum). (ii) In special case that the combined beam is inputted at the waist and the input power equals the critical power so that $z_s=0$ and $z_{p0}^{(\mathrm{rot})}=z_0$, both the beam width and the rotation velocity would remain constant upon propagation, and the rotating breather is reduced to the rotating soliton. (iii) Since the field at planes $z=(a+1/2)\pi z_{p0}^{(\mathrm{rot})}$ is the Fourier transform of the input field or the reverse [24], not only the beam width w but also the azimuthal orientation $\varphi(z)$ and the rotation velocity Ω at these planes are identical for different off-waist shifts.

If the rotating breather propagates from the entrance plane to a later plane, an arbitrary point of the beam in the entrance plane moves to another location in the transverse plane, keeping its individuality. According to Eqs. (7) and (20), we can obtain the trajectory equation of the point in the x-y plane:

$$r(z)=\frac{r_0\left\{1+\tan^2\left[\dfrac{\varphi(z)-\varphi_0}{B}\right]\right\}^{1/2}}{\left\{1+\left(\dfrac{z_0}{z_{p0}^{(\mathrm{rot})}}\right)^2\left[\tan\left(\dfrac{\varphi(z)-\varphi_0}{B}\right)+\dfrac{z_s}{z_0}\right]^2\right\}^{1/2}}, \tag{23}$$

where φ_0 and r_0 respectively represent the radial position and azimuthal orientation of the point at the waist of the input beam.

The motion of the point is determined by (i) the breath (or, in other words, the periodical variation in the beam width) of the breather, which results in the variation in radial position; and (ii) the rotation, which results in the variation in the azimuthal orientation. The width always breathes periodically with the period $\pi z_{p0}^{(\mathrm{rot})}$, whatever the input power and the off-waist distance are. On the other hand the rotation velocity and the azimuthal orientation of the point are crucially dependent on the azimuthally varied phase difference in x-y plane as well as the difference in the Gouy phase shift between the constituent beams, through the parameter B, which is determined by the indices l_1, p_1, l_2, and p_2. Therefore, as shown in Eq. (23), the parameter B plays an important role in the forming of the trajectory of the point.

Generally, if $z_s\neq 0$ and/or $P_0^{(\mathrm{rot})}\neq P_c$, the point undergoes different trajectories in x-y plane for different values of B [Figs. 8(b)–8(i)]. (i) If $B=1$, the trajectory shape is elliptical. In fact, in a new reference frame $X=x\cos[\varphi(z_m^{(0)})]+y\sin[\varphi(z_m^{(0)})]$, $Y=y\cos[\varphi(z_m^{(0)})]-x\sin[\varphi(z_m^{(0)})]$ (where $x=r\cos\varphi, y=r\sin\varphi$), we get

$$\frac{X^2}{\left(r_0\dfrac{w(z_m^{(0)})}{w_0}\right)^2}+\frac{Y^2}{\left(r_0\dfrac{w(z_m^{(1)})}{w_0}\right)^2}=1,$$

which is the standard equation for the ellipse. (ii) If $B=2$, the trajectory shape is ringed when $z_s=0$ and $P_0^{(\mathrm{rot})}=P_c$. With the increase in $|z_s|$ and/or deviation of the $P_0^{(\mathrm{rot})}$ from P_c, it first looks elliptical (but is not really an ellipse) [Fig. 8(c)], and then it becomes similar to the profile of an egg (not shown in Fig. 8). (iii) If $B=3,4,5,\ldots$, the trajectory spirals outward and inward alternately [Figs. 8(d)–8(f)]. If B is an odd (even) number, the trajectory spirals outward and inward twice (once) in a period. The variations in the azimuthal orientation of the point in a period are the same for $B=j$ and $B=2j$ $(j=3,5,7)$. (iv) If $B=1/k$ $(k=2,3,4,\ldots)$, the trajectory curves outward and inward alternately with the increase in the azimuthal angle φ, which yields a trajectory shape similar to a k-pointed star [Fig. 8(g)]. (v) If $B=k_1/k_2$ (k_1 and k_2 are relatively prime numbers; $k_1,k_2>1$), the trajectory is

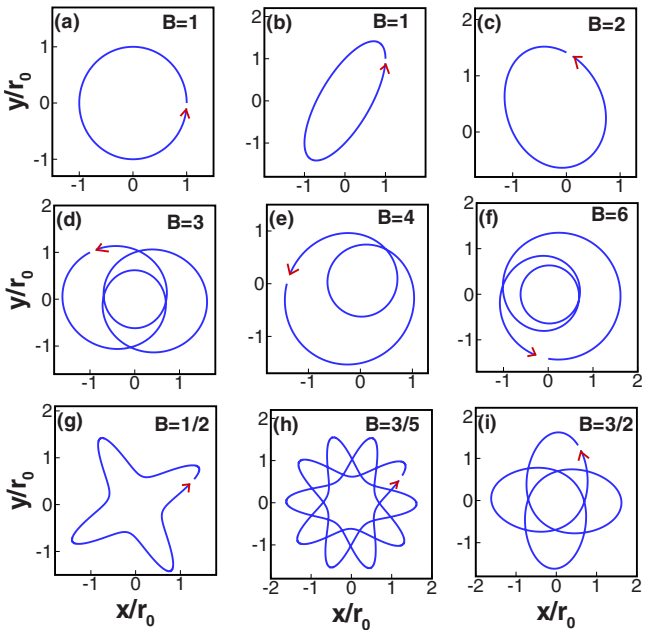

FIG. 8. (Color online) Trajectories of arbitrary individual point in x-y plane for different values of B. The off-waist distance is $z_s=0$ for (a) and is $z_s=-z_0$ for (b)–(i). $P_0^{(\mathrm{rot})}=P_c$; $\varphi_0=0$.

similar to a flower with $2k_2$ petals. If $k_1<k_2$, the trajectory curves outward and inward alternately [Fig. 8(h)], whereas if $k_1>k_2$, the trajectory always curves inward [Fig. 8(i)].

As shown in Eq. (23) and Fig. 8, in propagation the location of the point in x-y plane varies periodically. In a period, the variation in the azimuthal orientation of the point is

$$\Delta\varphi = 2n\pi,$$

where n is the minimum of the integers which satisfies $n=n'B/2$, with $n'=1,2,3\ldots$. The corresponding propagation distance is

$$\Delta z = \frac{\Delta\varphi}{B} z_{p0}^{(\mathrm{rot})} = \frac{2\pi n}{B} z_{p0}^{(\mathrm{rot})}.$$

On the other hand if the beam is inputted at the waist ($z_s=0$) and the input power $P_0^{(\mathrm{rot})}=P_c$, which ensures $z_{p0}^{(\mathrm{rot})}=z_0$, the breather reduces to a rotating soliton, and the point undergoes a ringed trajectory [Fig. 8(a)]. Under this condition, the variation in the azimuthal orientation of the point in a period is $\Delta\varphi=2\pi$, whatever B is, and the corresponding propagation distance is $\Delta z=2\pi z_{p0}^{(\mathrm{rot})}/B$.

IV. CONCLUSION

In conclusion, we have revealed that the off-waist input multiringed breathers and rotating breathers, which remain shape invariant and breathe sinusoidally, exist as two classes of breathers in SNN media. When the beams are inputted at the waist and the input power equals the critical power simultaneously, the multiringed breathers and the rotating breathers would reduce to multiringed solitons and rotating solitons, respectively. A multiringed breather can be created as a result of the superposition of two off-waist input even and odd Laguerre-Gaussian beams with identical parameters but a $\pm\pi/2$ phase difference between them. A rotating breather can be formed by superposition of two multiringed breathers with different indices; equivalently it can also be formed by superposition of four corresponding off-waist input Laguerre-Gaussian beams. Due to the dependence between the breath of the beam width and the periodically varied azimuthal orientation of the intensity pattern, every point within the beam cross section of a rotating breather undergoes novel trajectory during propagation.

ACKNOWLEDGMENTS

This research was supported by the National Natural Science Foundation of China (Grants No. 10674050 and No. 10804033), the Program for Innovative Research Team of Higher Education in Guangdong (Grant No. 06CXTD005), and the Specialized Research Fund for the Doctoral Program of Higher Education (Grants No. 20060574006 and No. 200805740002).

[1] H. L. Pecseli and J. J. Rasmussen, Plasma Phys. **22**, 421 (1980).
[2] F. Dalfovo and S. Giorgini, Rev. Mod. Phys. **71**, 463 (1999).
[3] C. Conti, M. Peccianti, and G. Assanto, Phys. Rev. Lett. **92**, 113902 (2004).
[4] M. Peccianti, K. A. Brzdakiewicz, and G. Assanto, Opt. Lett. **27**, 1460 (2002).
[5] C. Rotschild, O. Cohen, O. Manela, M. Segev, and T. Carmon, Phys. Rev. Lett. **95**, 213904 (2005).
[6] C. Rotschild, M. Segev, Z. Y. Xu, Y. V. Kartashov, L. Torner, and O. Cohen, Opt. Lett. **31**, 3312 (2006).
[7] A. Dreischuh, D. N. Neshev, D. E. Petersen, O. Bang, and W. Krolikowski, Phys. Rev. Lett. **96**, 043901 (2006).
[8] W. Krolikowski, M. Saffman, B. Luther-Davies, and C. Denz, Phys. Rev. Lett. **80**, 3240 (1998).
[9] O. Bang, W. Krolikowski, J. Wyller, and J. J. Rasmussen, Phys. Rev. E **66**, 046619 (2002).
[10] A. I. Yakimenko, V. M. Lashkin, and O. O. Prikhodko, Phys. Rev. E **73**, 066605 (2006).
[11] D. Buccoliero, A. S. Desyatnikov, W. Krolikowski, and Y. S. Kivshar, Opt. Lett. **33**, 198 (2008).
[12] D. Buccoliero, A. S. Desyatnikov, W. Krolikowski, and Y. S. Kivshar, Phys. Rev. Lett. **98**, 053901 (2007).
[13] A. W. Snyder and D. J. Mitchell, Science **276**, 1538 (1997).
[14] W. P. Zhong and Y. Lin, Phys. Rev. A **75**, 061801(R) (2007).
[15] M. Peccianti, C. Conti, G. Assanto, A. D. Luca, and C. Umeton, Appl. Phys. Lett. **81**, 3335 (2002).
[16] S. Lopez-Aguayo, A. S. Desyatnikov, and Y. S. Kivshar, Opt. Express **14**, 7903 (2006).
[17] W. Królikowski and O. Bang, Phys. Rev. E **63**, 016610 (2000).

[18] D. M. Deng and Q. Guo, Opt. Lett. **32**, 3206 (2007).
[19] A. V. Mamaev, A. A. Zozulya, V. K. Mezentsev, D. Z. Anderson, and M. Saffman, Phys. Rev. A **56**, R1110 (1997).
[20] N. I. Nikolov, D. Neshev, W. Królikowski, O. Bang, J. J. Rasmussen, and P. L. Christiansen, Opt. Lett. **29**, 286 (2004).
[21] S. Lopez-Aguayo and J. C. Gutiérrez-Vega, Opt. Express **15**, 18326 (2007).
[22] S. G. Ouyang, W. Hu, and Q. Guo, Phys. Rev. A **76**, 053832 (2007).
[23] Q. Guo, B. Luo, F. Yi, S. Chi, and Y. Xie, Phys. Rev. E **69**, 016602 (2004).
[24] D. Lu, W. Hu, and Q. Guo, e-print arXiv:0807.0701, Europhys. Lett. (to be published).
[25] A. Bekshaev and M. Soskin, Opt. Lett. **31**, 2199 (2006).
[26] S. M. Feng and H. G. Winful, Opt. Lett. **26**, 485 (2001).
[27] A. E. Siegman, *Lasers* (University Science, Mill Valley, CA, 1986).